

Wear and Corrosion Behavior of Zr-Doped DLC on Ti-13Zr-13Nb Biomedical Alloy

Prateek Kumar, P. Dilli Babu, L. Mohan, C. Anandan, and V.K. William Grips

(Submitted January 26, 2012; in revised form March 19, 2012; published online May 9, 2012)

Zirconium (Zr)-doped DLC was deposited on biomedical titanium alloy Ti-13Nb-13Zr by a combination of plasma-enhanced chemical vapor deposition and magnetron sputtering. The concentration of Zr in the films was varied by changing the parameters of the bi-polar pulsed power supply and the Ar/CH₄ gas composition. The coatings were characterized for composition, morphology, nanohardness, corrosion resistance in simulated body fluid (SBF) and tribological properties. X-ray photoelectron spectroscopy (XPS) studies on the samples were used to estimate the concentration of Zr in the films. XPS and micro-Raman studies were used to find the variation of I_D/I_G ratio with Zr concentration. These studies show that the disorder in the film increased with increasing Zr concentration as deduced from the I_D/I_G ratio. Nanohardness measurements showed no clear dependence of hardness and Young's modulus on Zr concentration. Reciprocating wear studies showed a low coefficient of friction (0.04) at 1 N load and it increased toward 0.4 at higher loads. The wear volume was lower at all loads on the coated samples. The wear mechanism changed from abrasive wear on the substrate to adhesive wear after coating. The corrosion current in SBF was unaffected by the coating and corrosion potential moved toward nobler (more positive) values.

Keywords corrosion, DLC, titanium alloy, wear, XPS

1. Introduction

Amorphous hydrogenated diamond-like carbon (DLC) is a class of metastable form of amorphous carbon with excellent mechanical properties like high hardness, low coefficient of friction, chemical inertness, and biocompatibility (Ref 1-5). These properties of DLC are due to its tetrahedral bonding structure similar to diamond with some C-C bonds replaced by C-H bonds and with a significant percentage of sp^3 -bonded carbon (Ref 5). DLC is composed of cross-linked structure with isolated nanoclusters of covalently bonded sp^2 and sp^3 carbon atoms. The advantage of this allotrope of carbon is that the ratio of sp^2/sp^3 can be varied in it by varying the deposition parameters. The ratio of the sp^3/sp^2 carbon atoms is one of the most important factors that determine the quality of the DLC films. In general, higher this ratio the closer the DLC film properties approach those of diamond (Ref 6, 7). DLC coatings can be deposited with hardness in the range of 10-70 GPa depending upon deposition techniques (Ref 5). DLC coatings have found widespread use in magnetic storage devices (Ref 5) as a protection against head crashes, electronic applications (Ref 8-10), tooling components like drill bits (hardness and wear resistance) and automobile components (reduces friction)

(Ref 11). Also, they find applications as biocompatible coatings for different biomedical applications (Ref 4). The adhesion of DLC to several substrates is poor due to high internal stress present in them, thus limiting their application (Ref 12, 13). But, by doping or depositing in graded interlayer with silicon, nitrogen, or metals like chromium, zirconium, titanium, and niobium, the adhesion of DLC can be improved (Ref 14-22). Among the metals, transition metals such as zirconium, titanium, tantalum, and niobium are known to be biocompatible. Therefore, doping the DLC coating with these metals will have synergistic effect of improving the adhesion as well as biocompatibility of DLC coatings. Doping may, however, decrease hardness and modulus of elasticity, leading to higher wear rates. Therefore, to reduce wear, the films can be graded in a way that dopant concentration near the interface is higher and it is reduced gradually to a small value near the surface so that adhesion is maintained without compromising the hardness (Ref 23). Due to the gradual transition, the potential places for crack propagation is also minimized (Ref 18). Thus, DLC can be deposited on substrates on which it does not adhere well or thicker coatings cannot be deposited.

Titanium alloys are widely used in biomedical applications due to their low density, good mechanical properties, high strength-to-weight ratio, and corrosion resistance. Ti-13Nb-13Zr is a near beta titanium alloy with a modulus of 80 GPa that is lower than conventional Ti-6Al-4V or Ti6Al-7Nb (114 and 104 GPa, respectively) but is closer to that of femoral bone (≈ 30 GPa). Therefore, it finds increasing usage in load-bearing bio-implants. However, like other titanium alloys, it also has poor tribological properties (Ref 8, 9). Surface modification techniques such as plasma nitriding, ion implantation, or over-layer deposition can be used to improve the tribological properties. However, any surface modification treatments should not deteriorate the corrosion resistance of the alloys. As discussed above, DLC coatings, with good tribological

Prateek Kumar, P. Dilli Babu, L. Mohan, C. Anandan, and V.K. William Grips, Surface Engineering Division, CSIR-National Aerospace Laboratories, Old Airport Road, P.O. Box 1779, Bangalore 560 017 Karnataka, India. Contact e-mail: canandan@nal.res.in.

properties and biocompatibility can be used for enhancing the tribological properties of titanium alloys. In this paper, the results of evaluation of tribological and corrosion properties of Zr-doped DLC on Ti-13Nb-13Zr titanium alloy are presented.

2. Experimental Details

2.1 Sample Preparation

In this study, three different substrates were used. Silicon wafers (100) were cut into appropriate sizes for x-ray photoelectron spectroscopy (XPS), Nanohardness testing, atomic force microscopy, and micro-Raman studies, and cleaned in acetone and IPA ultrasonically. Glass slides were cut and after cleaning them a portion was masked for thickness measurement by profilometer. Titanium alloy Ti-13Zr-13Nb,

ASTM -F1713-08 grade was cut into square samples of $1.5 \times 1.5 \times 0.2$ cm. The samples were grounded by silicon carbide emery papers of different grit sizes to smoothen the surface and then polished to mirror-like finish with $0.03 \mu\text{m}$ alumina powder mixed in distilled water. The polished samples were then ultrasonically cleaned for 15 min each in acetone and IPA. The roughness of the samples after polishing was $0.1 \mu\text{m}$. These samples are then loaded in the chamber for coating.

2.2 Deposition System

The chamber was pumped down to a base vacuum of 3×10^{-6} mbar by a turbo molecular pump backed with a rotary pump. After reaching the base pressure, the chamber and the gas lines were purged with process gases. The source gases CH_4 , Ar, and H_2 were introduced in the chamber by a shower head-type distributor and the flow rates were controlled by MKS make

Table 1 Deposition parameters for pulsed DC power supply

Sample no.	Set parameters				Positive channel		Negative channel		Substrate bias, V
	Bias V, V	Bias I, A	Bias power, kW	Bias F, kHz	Pulse on+, μs	Pulse off+, μs	On-, μs	Off-, μs	
1	300	0.6	0.6	10	85	5	5	5	-145
2	300	0.6	0.6	10	70	20	5	5	-145
3	300	0.6	0.6	10	75	15	5	5	-145
4	300	0.6	0.6	10	50	40	5	5	-145
5	300	0.6	0.6	10	60	30	5	5	-145
6	300	0.6	0.6	50	6	3	8	3	-145
7	300	0.6	0.6	50	5	5	5	5	-145
8	400	0.6	0.6	50	7	3	7	3	-80
9	400	0.4	0.6	50	7	3	7	3	-145
10	400	0.6	0.6	50	5	5	5	5	-145
11	400	0.6	0.6	50	5	5	7	3	-145

Table 2 Parameters for the gas composition and the deposition time

Sample no.	Gas Pr, μbar	Zr interlayer		Zr-doped DLC		Pure DLC		Total duration, min
		Ar, sccm	Ar duration, min	Ar:CH ₄ , sccm	Duration, mins	CH ₄ :H ₂ , sccm	Duration, min	
1	11	10	5	7:3	30	35
2	11	10	5	7:3	30	35
3	11	10	5	7:3	30	35
4	11	10	5	7:3	30	35
5	11	10	5	7:3	30	35
6	11	10	5	7:3	30	35
7	8	10	5	5:5	30	35
8	11, 2	10	5	7:3	30	6:4	10	45
9	11, 3	10	10	7:3	45	9:1	35	90
10	8	10	5	7:3, 5:5	10, 20	35
11	11	10	5	7:3, 5:5	10, 20	35

Table 3 Variation of I_D/I_G ratio, nanohardness, and Young's modulus with Zr concentration

Sample no.	%Zr	I_D/I_G ratio of DLC film on Si	sp^2/sp^3 from XPS	Hardness, GPa	Vickers hardness	Young's modulus, GPa
1	38.2	1.15	1.70	15.15 ± 0.64	1403.3 ± 59.83	156.7 ± 9.33
2	12.9	1.08	1.63	13.64 ± 0.54	1263.8 ± 50.12	162.9 ± 6.59
6	2.7	1.07	0.77	14.66 ± 0.68	1358.5 ± 63.03	186.4 ± 8.18
8	0.12	0.89	0.41	16.83 ± 0.77	1559.3 ± 72.73	149.6 ± 7.71

mass flow controllers. Pressure in the chamber was monitored by a MKS make Baratron and controlled by a throttle valve. Zr was sputtered using a magnetron sputtering gun. The magnetron sputtering gun was powered by a bi-polar pulsed DC power supply, supplied by MAGPULS Stromversorgungs Systeme GmbH, Sinzheim, Germany. The plasma was generated by 50 W RF power at a frequency of 13.56 MHz by inductive coupling and the substrates were negatively biased. Sputtering of Zr was carried out at different pulse “ON” and “OFF” times and at different argon-to-methane ratios to vary the Zr concentration in the coating. Prior to deposition, the samples were etched in hydrogen plasma for 15 min. Table 1 gives the deposition parameters for the pulsed power supply and Table 2 the gas composition and other parameters.

2.3 Characterization Techniques

The coatings were characterized by confocal micro-Raman using DILOR-JOBIN-YVON SPEX made LABRAM 010A with He-Ne laser source having wavelength of 632.8 nm. XPS analysis was carried out using SPECS make XPS system. The spectra were obtained using 100 W Al K α radiation in the as-received condition and also after 3 min of sputter etching with 1 keV argon ions. The C1s and Zr3d core level spectra were obtained at a pass energy of 25 eV. The atomic percentage of Zr in the coatings was estimated using the area under the C1s and Zr3d core level spectra and the respective XPS relative sensitivity factors (RSF). Surface topography of the coatings was obtained by Surface Imaging Systems AFM on a 10 \times 10 μ m area and also with Carl Zeiss SUPRA 10VP field emission electron microscope (FESEM). Elemental analysis was performed by EDS using Oxford instruments Inca Penta FET X 3 EDS attachment to FESEM. Nanohardness was measured using a Nanohardness Tester (CSM instruments) with a Berkovich Diamond indenter at 5 mN load. Wear studies were carried out in a reciprocating-type wear tester (Model CM 9084 DuCom) according to ASTM G133-02 standards (Ref 24). However, these tests are not in full compliance with the provisions of Test Method G 133, Procedure A, because the normal force in these experiments was 1, 2, and 5 N instead of

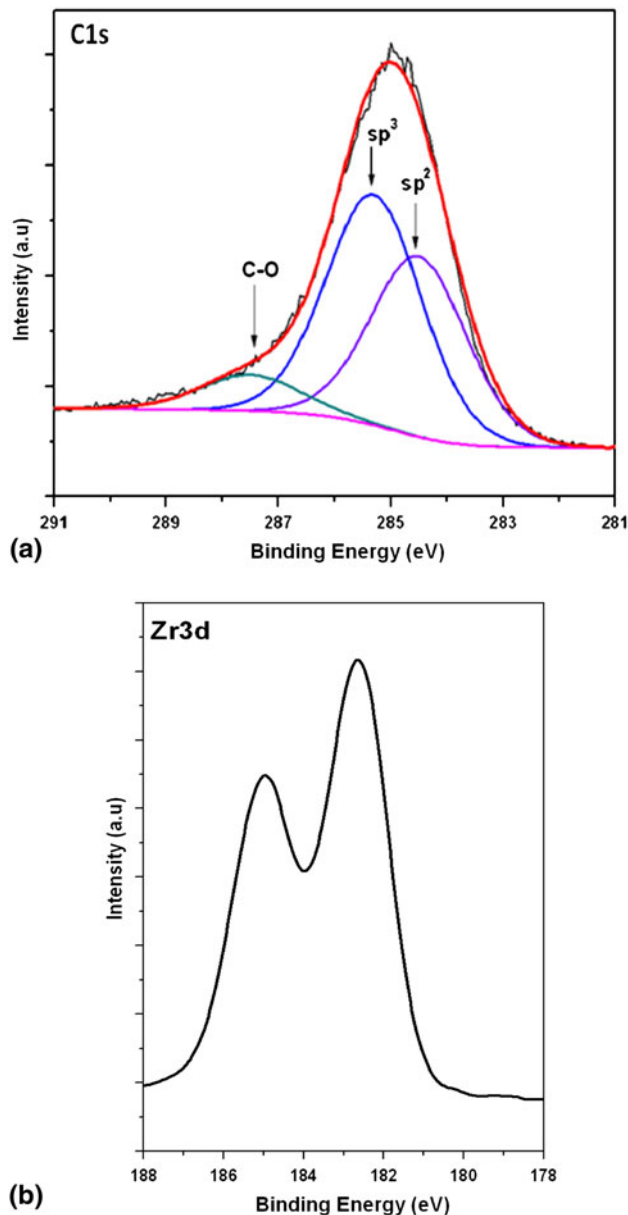


Fig. 1 (a) XPS spectrum of C1s core level along with the fitted curves and (b) XPS spectrum of Zr 3d core level

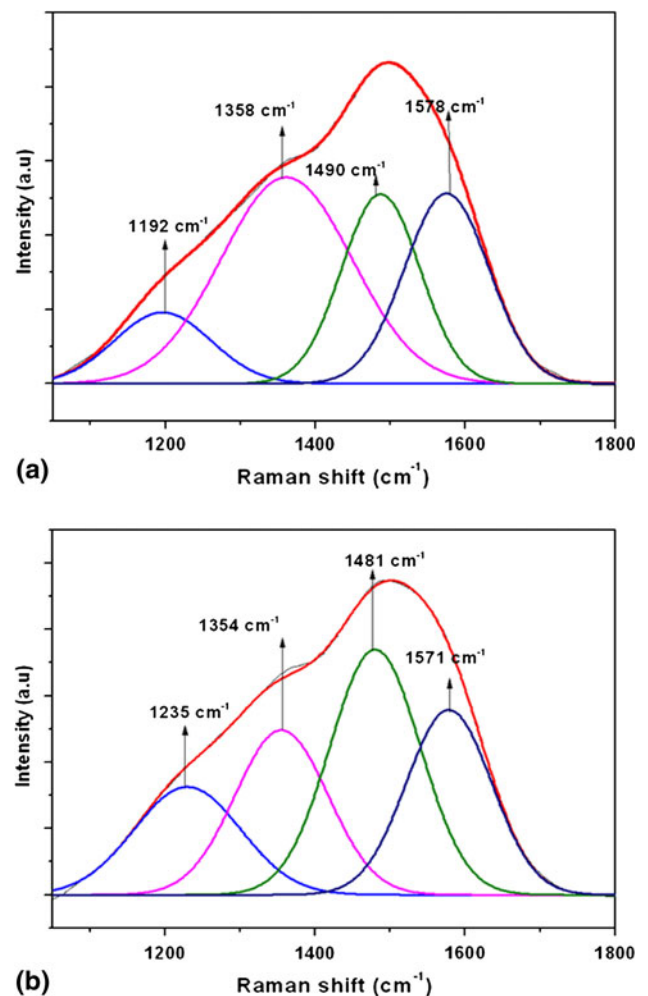


Fig. 2 Raman spectra of Zr-doped DLC coatings. (a) 38% Zr and (b) 0.1% Zr

25.0 N as prescribed by the standard. Also, the stroke length was 10 mm and an alumina ball of 6 mm diameter was used as the counter surface. Further, the experiments were carried out at a frequency of 100 Hz/min for 20 min. After the experiments, the samples were examined for wear profile by a profilometer. The wear loss was calculated from the cross-sectional area of the wear profile according to ASTM G133-02 method (paragraph-9.3.1). Optical micrographs of the wear tracks on the samples and on the alumina balls were taken at different magnifications. The samples were also examined by micro-Raman for changes in surface composition.

Electrochemical studies on the substrate and DLC samples were conducted using CHI604D Electrochemical Workstation. The conventional three-electrode glass cell was used to carry out the electrochemical studies. The test was conducted in 200 mL of Hank's solution which simulates the body fluid (SBF). The chemical composition of the Hank's solution is as follows: 0.185 g CaCl_2 (1.258 mol), 0.4 g KCl (0.00536 mol), 0.06 g KH_2PO_4 (0.0004 mol), 0.1 g $\text{MgCl}_2 \cdot 6\text{H}_2\text{O}$ (0.00049 mol), 0.1 g $\text{MgSO}_4 \cdot 7\text{H}_2\text{O}$ (0.00041 mol), 8.0 g NaCl (0.137 mol), 0.35 g NaHCO_3 (0.00417 mol), 0.48 g Na_2HPO_4 (0.00269 mol), and 1.00 g D-glucose in 1 L of milli-Q water. The pH of the solution was adjusted with 1 M HCl to 7.2-7.6 and the experiments were carried out at room temperature. The sample was treated as the working electrode. Pt foil and saturated calomel electrode (SCE) were used as counter and reference electrodes, respectively. The reference electrode was connected to a Luggin capillary and the tip of the Luggin capillary was kept very close to the surface of the working electrode to minimize IR drop. The samples were immersed in the Hank's solution for an hour to establish the open circuit potential (E_{OCP}) or steady state potential. Potentiodynamic polarization studies were carried out in a potential range of ± 200 mV about the OCP. The Tafel plots obtained after the measurements are represented in the form of potential vs. log (i)

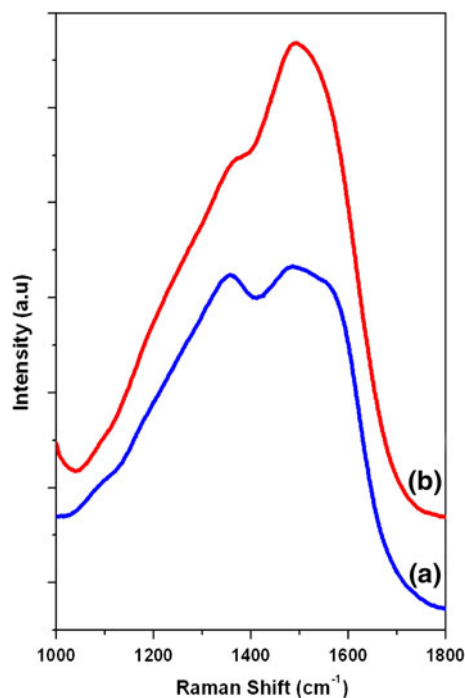


Fig. 3 Raman spectra of DLC-coated sample on (a) Ti-13Nb-Zr and (b) Si substrate

plot. The corrosion potential, E_{corr} , and corrosion current, I_{corr} , were deduced from the Tafel plot.

3. Results and Discussions

It was found that pure DLC did not adhere to titanium substrates without an interlayer but adhered to Si substrate. Therefore, an interlayer of pure zirconium was necessary for good adhesion to the substrates. Also, undoped DLC with interlayer started peeling off from the Ti substrates after some time. However, Zr doping and depositing the films in graded Zr composition improved the adhesion to the titanium substrates. Table 3 shows the Zr at.% obtained from XPS analysis. The percentage of Zr in the films varied from 39 to 0.1 at.% depending on the process gas composition and the pulse ON/OFF times of the bi-polar pulsed power supply. As Zr incorporation was lower at 50%Ar dilution as compared to that at 70% dilution, most of the experiments were carried out at 70% dilution (Ref 25, 26). The thickness of the films was obtained from profilometry by masking a portion of the glass substrate. The thickness of the films ranges from 200 to 500 nm for Zr-doped DLC for various run numbers.

Figure 1(a) and (b) shows the C1s and Zr3d core level spectra, respectively. C1s spectrum is fitted with Gaussian peaks to find out the sp^2/sp^3 ratio (Ref 6). The Zr concentration and the sp^2/sp^3 ratio for DLC coatings for some of the samples are given in Table 3.

The Raman spectra for Zr-doped DLC coatings on silicon are shown in Fig. 2(a) for high Zr concentration and in Fig. 2(b) for low Zr concentration. The spectra were fitted with Gaussian peaks to estimate the I_D/I_G ratio. In general, two peaks are used to fit Raman spectra of DLC coatings in the 1100 to 1700 cm^{-1} range. However, it has been suggested that a good fit of the Raman spectra of DLC needs four Gaussian peaks (Ref 27, 28). The peaks at 1150 and 1450 cm^{-1} correspond to the sum and difference of the C=C chain stretching and C-H wagging modes of trans polyacetylene and the other resonating double bond (Ref 29). The peak at 1150 cm^{-1} is accompanied by its companion mode at 1450 cm^{-1} . The peak located at a wave number of 1360 cm^{-1} corresponds to disordered A_{1g}

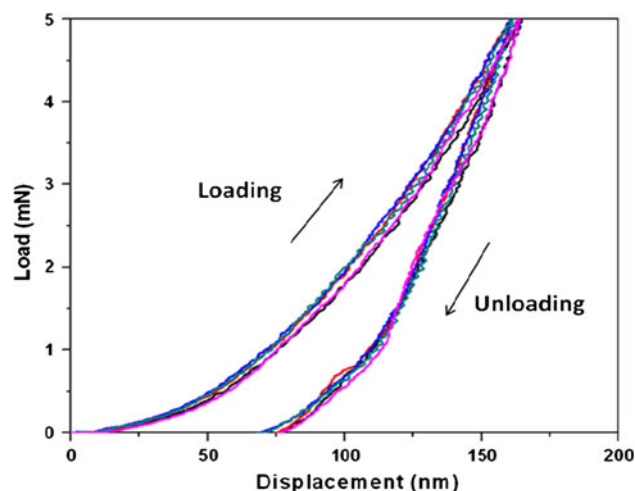


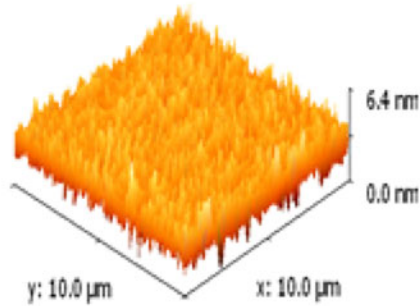
Fig. 4 Load versus displacement curve for five different indentations

breathing sp^2 carbon bonds and is known as D-peak. The G-peak located at a wave number of 1550 cm^{-1} corresponds to the e_{2g} stretching of sp^2 carbon bonds (Ref 30, 31). The G-peak

is due to the bond stretching of sp^2 bonded carbon in both ring and chain carbon compounds. In this study, the Raman spectra of Zr-doped DLC are fitted with four peaks and the ratio of the

10X10 microns Area roughness

Parameters	
Average value:	2.984 nm
Minimum:	0.000 nm
Maximum:	6.411 nm
Median:	2.985 nm
Ra:	0.477 nm
Rms:	0.602 nm
Skew:	0.0386
Kurtosis:	0.255
Surface area:	100.0552 μm^2
Projected area:	100.0000 μm^2



Roughness of 3 profiles

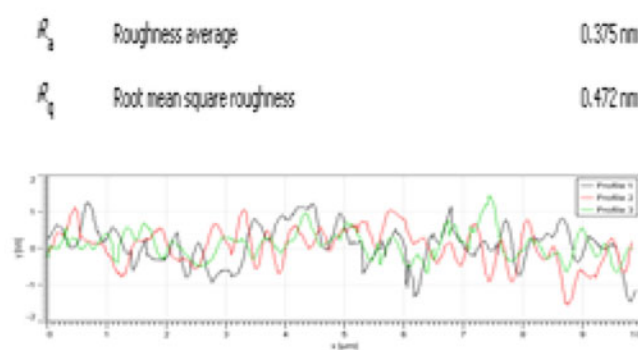


Fig. 5 AFM image and line profiles of typical Zr-doped DLC coating on silicon substrate on $10 \times 10\ \mu\text{m}$ area

Table 4 Average and RMS roughness of coated Si samples

Sample no.	Average roughness (Ra), nm	Root mean square (RMS), nm
Si substrate	0.25	0.32
1	0.50	0.59
8	0.40	0.50
9	0.37	0.46
10	0.34	0.43
11	0.37	0.47

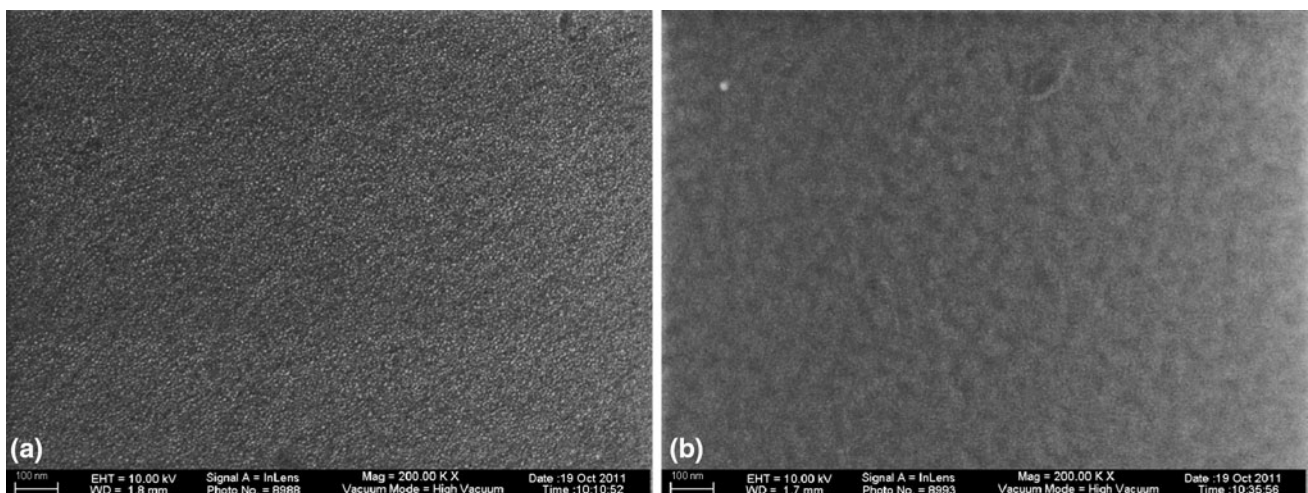


Fig. 6 FESEM images of Zr-doped DLC coating on silicon substrate. (a) 38 at.% Zr and (b) 0.1 at.% Zr

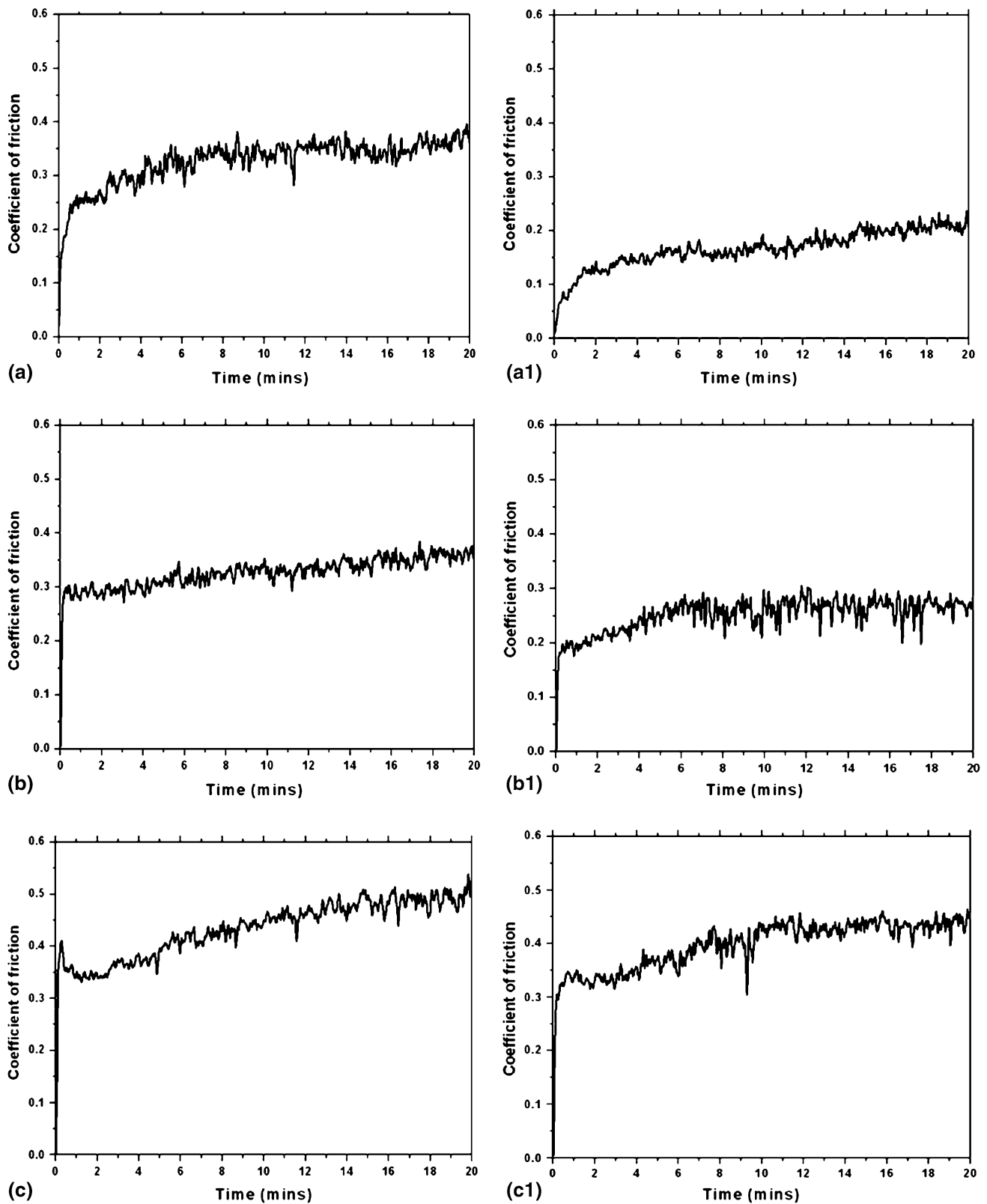


Fig. 7 Friction coefficients versus time on (a) substrate (a1) Zr + DLC coated samples for 1 N load, (b) substrate (b1) Zr + DLC coated samples for 2 N load, (c) substrate (c1) Zr + DLC coated samples for 5 N load

amplitudes of the D peak at 1360 cm^{-1} to the G peak at 1550 cm^{-1} is used to estimate the I_D/I_G ratio (Ref 32). The I_D/I_G values represent the degree of disorder in the carbon network. The I_D/I_G ratios lie in between 0.8 and 1.2 for

different Zr-doped DLC coatings and are listed in Table 3. It can be seen from the table that metal incorporation increases the D-peak and hence I_D/I_G ratio at higher Zr concentration. The Raman spectra of DLC coating on Ti-13-13 alloy and Si

substrate are compared in Fig. 3 and shows that on Ti-13-13 metallic substrates the disorder in the coating increases.

Nanohardness measurements were carried out on Zr-doped DLC-coated silicon samples at 5 mN load. Figure 4 shows five indentation curves taken at different locations on the sample and shows the uniformity of the coating hardness. The average hardness of the coating was 15 GPa and Young's modulus was 160 GPa. The I_D/I_G ratios, estimated from Raman spectra and from XPS, hardness and Young's modulus of different DLC coatings with different Zr concentrations are shown in Table 3. Though there is a difference in the I_D/I_G ratios obtained by Raman and XPS methods, the trend is similar in the sense that the ratio increases with increasing Zr concentration. The difference in the I_D/I_G ratio obtained between the two methods

may be due to the fact that XPS is a surface-sensitive technique with a sampling depth of few nanometers which is much lower than that of micro-Raman technique. It can be seen that I_D/I_G ratio increases with increase in Zr concentration and thereby suggests that the disorder in the material increases with increasing metal atom concentration in the DLC coating (Ref 31). Nanohardness values do not show any clear dependence on Zr concentration. However, previous works have reported softening of DLC coatings with metal doping (Ref 14-22). This has been attributed by the authors to the increase in sp^2 disordered phase due to metal doping in the films.

AFM image and line profiles of a typical DLC coating on silicon substrate are shown in Fig. 5. Table 4 lists the roughness values of the silicon substrate and DLC-coated

Table 5 Coefficient of friction of substrate and coating under loads of 1, 2, and 5 N

	Average coefficient of friction under load, N		
	1	2	5
Ti-13-13 substrate	0.34	0.42	0.48
1	0.04	0.30	0.40
9	0.05	0.35	0.40
10	0.07	0.25	0.30

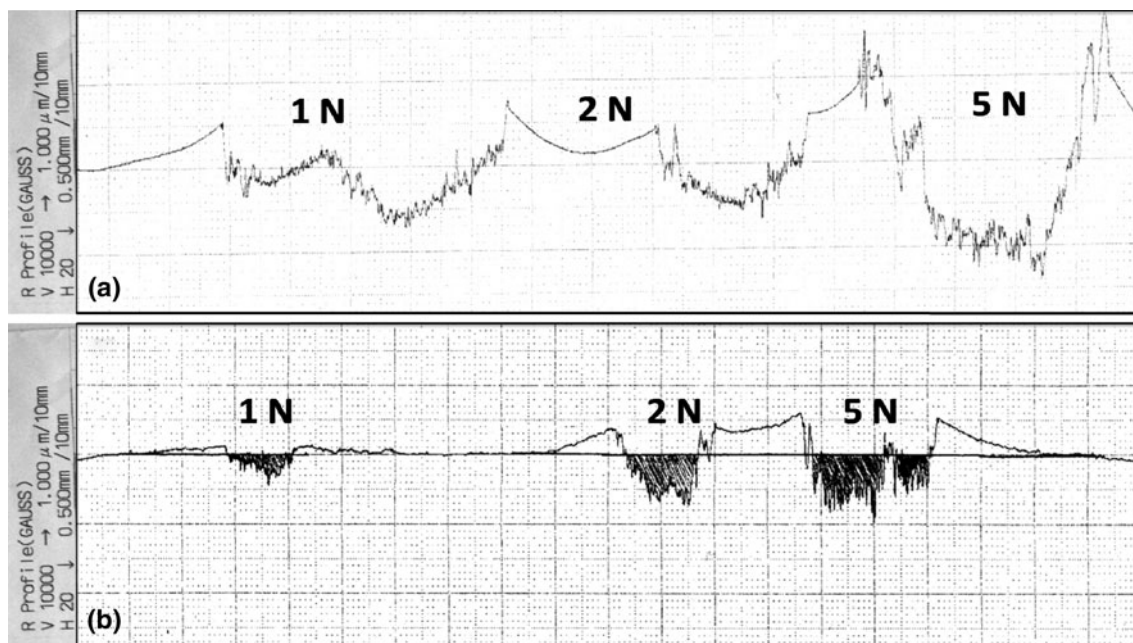


Fig. 8 Profiles of the wear tracks (a) on Ti-13-13 substrate and (b) coated substrate under 1, 2, and 5 N loads

Table 6 Wear volume for substrate and DLC-coated substrate

	Wear volume, mm ³ , under different loads, N		
	1	2	5
Ti-13-13 substrate	2.5×10^{-2}	3×10^{-2}	4.6×10^{-2}
1	5×10^{-3}	2.05×10^{-2}	4×10^{-2}
9	8×10^{-3}	2.6×10^{-2}	4×10^{-2}
10	6×10^{-3}	2.5×10^{-2}	2.65×10^{-2}

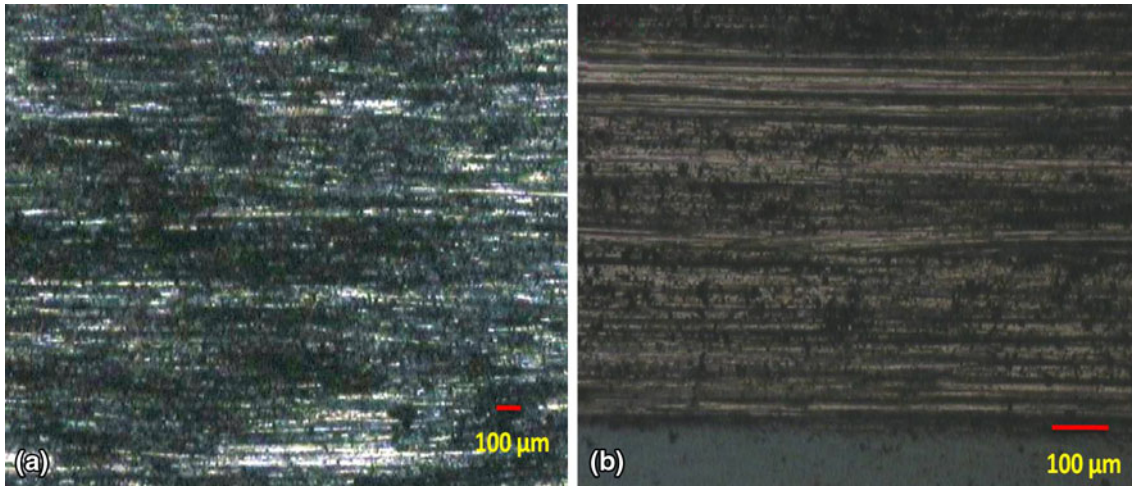


Fig. 9 Optical micrographs of the wear tracks at 5 N load. (a) Substrate and (b) coated sample

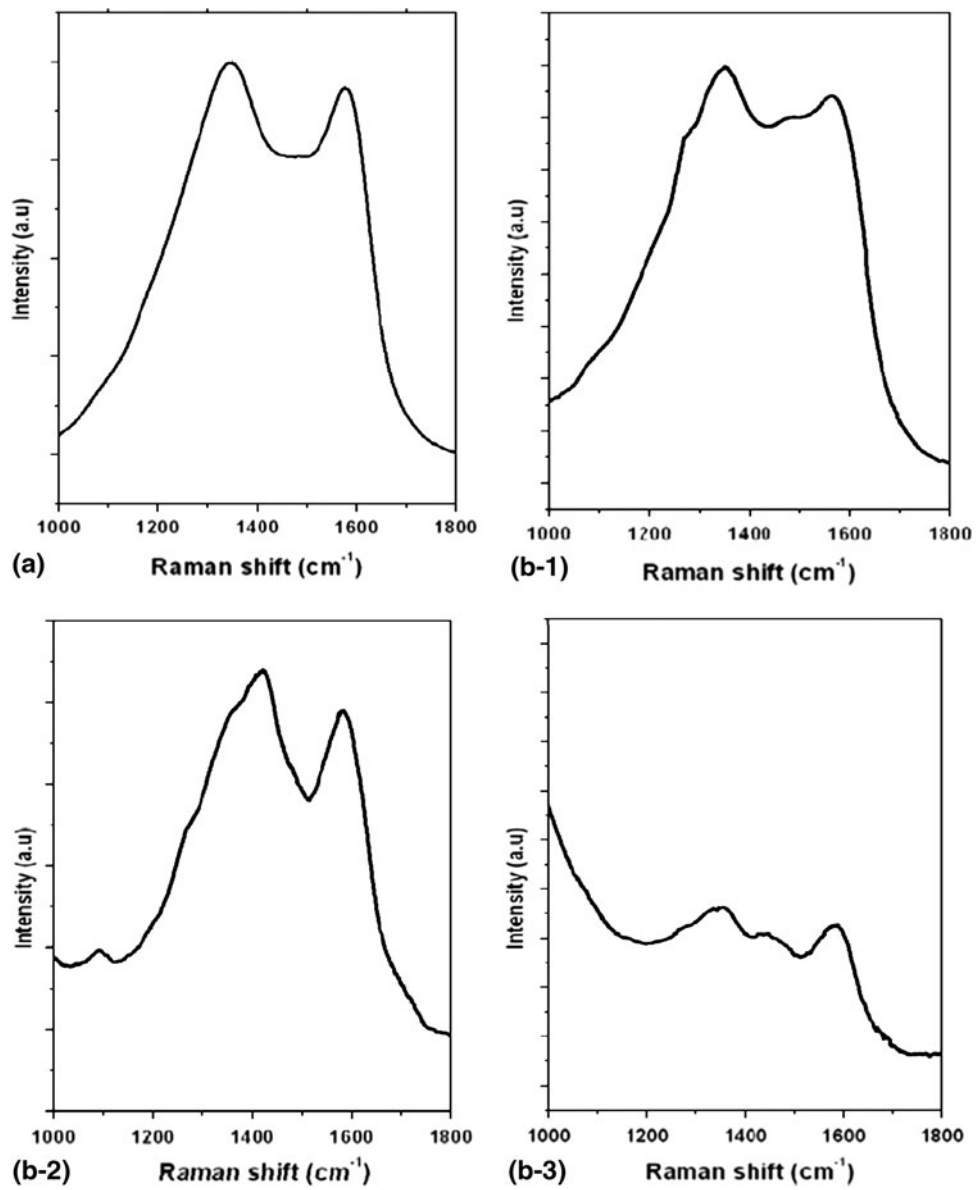


Fig. 10 Raman spectra of Zr + DLC on coated sample. (a) Before and (b) after wear testing (b-1) 1 N, (b-2) 2 N, and (b-3) 5 N loads

silicon samples. Line profiles at three different places on the coatings are also shown in Fig. 5, which shows the overall smoothness of the coatings on the substrates. FESEM images, at 200,000 magnifications, of the coatings are shown in Fig. 6(a) and (b) for two different Zr concentrations. The coatings show a compact and dense microstructure. Coating with lower Zr concentration shows a smoother surface as in Fig. 6(b) compared to higher Zr concentration in Fig. 6(a).

Figure 7(a) to (c) shows the evolution of friction coefficient for different loads in a linear reciprocating wear test. The average values of friction coefficient (FC) for the Ti-13Zr-13Nb substrate and Zr-doped DLC-coated substrates are given in Table 5. On the Ti-13-13 substrate, the friction coefficient is initially low but increases to 0.34-0.48. The coated substrates exhibit a low friction coefficient of around 0.03 at 1 N load and a higher value of 0.4 at higher loads. Friction coefficient on Zr-doped DLC is very low for a load of 1 N. However, for higher loads the friction coefficient increased with time and was almost equal to that of substrate after 20 min. Thus, the coating considerably reduced friction for low loads and for higher loads once the coating was removed the friction coefficient reaches that of substrate.

The profile of the wear tracks on the substrate is shown in Fig. 8(a) and that on Zr-doped DLC containing 0.12 at% Zr in Fig. 8(b). The wear track area is estimated by calculating the area of the shaded region below the mean coating level as shown in Fig. 8(b). The wear volume is then calculated by multiplying the wear area and the track length in accordance with ASTM G 133 standards. Wear volumes of substrate and coatings at loads of 1, 2, and 5 N are given in Table 6. For coated samples, with 1 N load the wear loss was negligible and was around 0.006 mm³. With 2 N load the wear volume was about 0.02 mm³ and with 5 N load it was around 0.04 mm³. Table 6 shows that the DLC coatings considerably reduce wear of the substrate and also reduce the friction coefficient, especially at low loads. Optical micrographs of the wear tracks on the samples and on the substrate are shown in Fig. 9. The optical micrographs of the wear tracks on the substrate shows an abrasive wear track with rough wear marks. On the coated sample the optical micrograph shows a smoother surface typical of adhesive wear and the friction coefficient curve is also smoother. The wear behavior also changes from abrasive wear on the substrate to adhesive wear on the coated substrate.

Micro-Raman spectra were taken on the DLC coatings on the wear tracks on the coated substrates and alumina ball used for wear tests. These are shown in Fig. 10(a) and (b) for the untreated coating and on wear tracks, respectively, on the sample for 1, 2, and 5 N loads. As is seen from the figure, Raman spectra change with the loads. At 1 and 2 N there is no change in the spectra, but at 5 N the coating thickness is small as can be seen from the intensity. This shows that the coating has been removed. The Raman spectra on the wear scar on the alumina ball did not show the presence of any DLC on the surface, probably due to its low thickness; however, it appeared darker in color after wear testing.

The potentiodynamic polarization curves of the substrate and Zr-doped DLC samples in Hank's solution (pH between 7.2 and 7.6) are shown in Fig. 11. The electrochemical parameters, namely, corrosion potential (E_{corr}) and corrosion current density (i_{corr}), obtained for the substrate and treated samples are given in Table 7. The polarization resistance, R_p , was estimated from the anodic and cathodic slopes and is also listed in the Table 7. From the table it is evident that the i_{corr} value obtained for the

substrate is of the order of 0.003 and 0.002 $\mu\text{A}/\text{cm}^2$ for Zr-doped DLC samples. Also, as is seen from the table, the polarization resistance is about $1 \times 10^7 \Omega \cdot \text{cm}^2$ for the treated samples higher than that for substrate. The E_{corr} values shifted to more positive values in the case of DLC-deposited samples. This shows that Zr-doped DLC has similar or better corrosion property as compared to the substrate in the potential region of interest.

Further, the composition of the corrosion-tested sample was obtained by EDS. The EDS data in Table 8 show the presence of O, Na, Cl, P, and Ca. Figure 12 shows XPS spectra of the sample after corrosion testing which shows the presence of Ca, Cl, and P. Sputter cleaning the sample by 3 min removes the peaks. This shows that the coated sample is bioactive in that apatite growth can occur on the Zr-doped DLC-coated samples. Thus, the wear and the corrosion studies show that Zr-doped

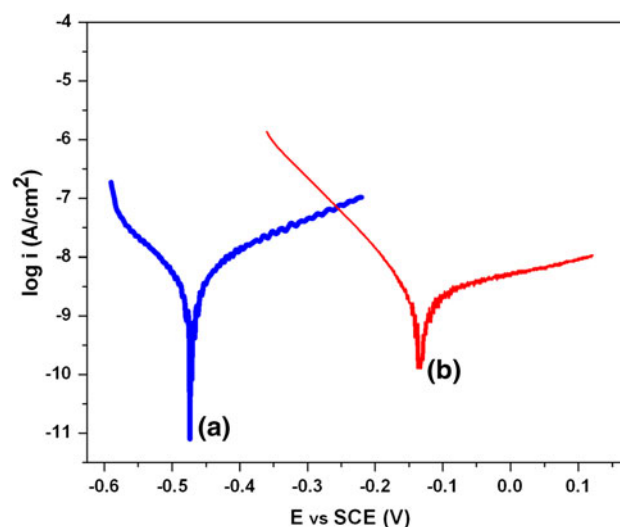


Fig. 11 Tafel plots for (a) substrate and (b) Zr-doped DLC-coated samples

Table 7 Potentiodynamic polarization results of substrate and Zr + DLC-deposited samples

	E_{corr} , V	i_{corr} , $\mu\text{A}/\text{cm}^2$	R_p , $\Omega \cdot \text{cm}^2$
Substrate	-0.472	0.003	5.92E^6
Zr-doped DLC (1)	-0.130	0.002	1.12E^7

Table 8 EDS results of Zr-DLC-deposited samples after corrosion

Element	wt. %	at. %
Ti	55.33	37.59
Zr	12.29	4.39
Nb	10.66	3.73
C	15.49	41.96
O	5.89	11.98
Ca	0.16	0.13
P	0.01	0.01
Na	0.11	0.16
Cl	0.06	0.05

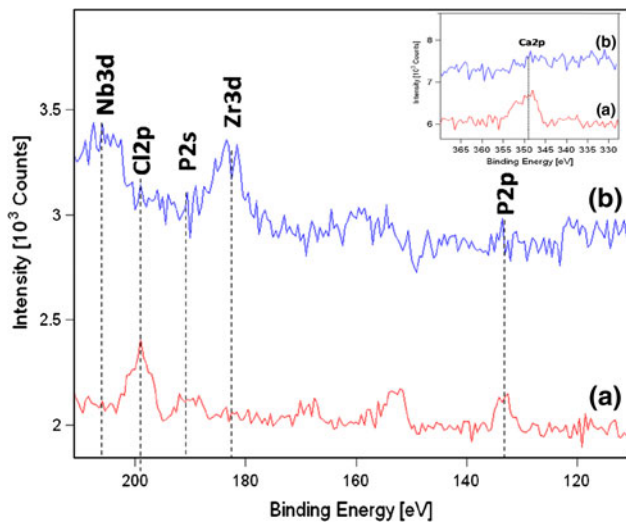


Fig. 12 XPS spectrum with P2p, Cl2p peaks after corrosion test. (a) Before and (b) after sputter etching (inset shows Ca2p region)

DLC coatings can be used as biocompatible coating to improve the tribological properties of Ti-13Zr-13Nb alloys.

4. Conclusions

Zr-doped DLC has been deposited on Ti-13Zr-13Nb biomedical titanium alloy. The deposition of Zr underlayer and Zr doping improves the adhesion of DLC coatings on otherwise difficult to coat substrate. Zr concentration can be varied from 39 to 0.1 at.% by varying the deposition parameters. The increased I_D/I_G ratio, determined from micro-Raman shows that metal doping increases the disorder in the DLC coatings. No clear dependence of hardness on Zr concentration was observed. Wear studies show a low friction coefficient of 0.04 at 1 N load and an order of magnitude lower wear rate of the coated substrates as compared to uncoated one. Potentiodynamic polarization studies show that the coated sample has the similar corrosion property as that of uncoated sample. Also, the coating is biocompatible as growth of apatite has been observed on the coated sample after corrosion testing in Hank's solution. Thus, Zr-doped DLC can be used as biocompatible coating to improve the tribological properties of Ti13Zr13Nb.

Acknowledgments

The work was carried out under the CSIR network project on Nanostructured Advanced Materials NWP-51-02. The authors would like to thank the Director, National Aerospace Laboratories, Bangalore for his support and permission to publish the work. The authors would like to thank Mr. Siju, Mr. N. T. Manikandanath, Mr. Praveen and Mr. Muniprakash for FESEM, micro-Raman, NHT, AFM and Wear studies.

References

1. R. Hauert, A Review of Modified DLC Coatings for Biological Applications, *Diam. Relat. Mater.*, 2003, **12**, p 583–589

2. J. Fontaine, C. Donnet, and A. Erdemir, Fundamentals of the Tribology of DLC Coatings, *Tribology of Diamond-Like Carbon Films: Fundamentals and Applications*, C. Donnet and A. Erdemir, Ed., Springer, New York, 2008, p 139–154
3. L.A. Thomson, F.C. Law, N. Rushton, and J. Franks, Biocompatibility of Diamond-Like Carbon Coating, *Biomaterials*, 1991, **12**, p 37–40
4. A. Grill, Diamond-Like Carbon Coatings as Biocompatible Materials—An Overview, *Diam. Relat. Mater.*, 2003, **12**, p 166–170
5. J. Robertson, Diamond-Like Amorphous Carbon, *Mater. Sci.*, 2002, **37**, p 129–281
6. P. Merel, M. Tabbal, M. Chaker, S. Moisa, and J. Margot, Direct Evaluation of the sp^3 Content in Diamond-Like-Carbon Films by XPS, *Appl. Surf. Sci.*, 1998, **136**, p 105–110
7. Alfred. Grill, Diamond-Like Carbon: State of the Art, *Diam. Relat. Mater.*, 1999, **8**, p 428–434
8. E. Alakoski, V.-M. Tiainen, A. Soininen, and Y.T. Konttinen, Load-Bearing Biomedical Applications of Diamond-Like Carbon Coatings—Current Status, *Open Orthop. J.*, 2008, **2**, p 43–50
9. K. Budinski, Tribological Properties of Titanium Alloys, *Wear*, 1991, **151**, p 203–217
10. J. Robertson, Improving the Properties of Diamond-Like Carbon, *Diam. Relat. Mater.*, 2003, **12**, p 79–84
11. N. Cao, Z.-Yi. Fei, Y.-X. Qi, W.-W. Chen, L.-L. Su, and Q. Wang, Characterization and Tribological Application of Diamond-Like Carbon (DLC) Films Prepared by Radio-Frequency Plasma-Enhanced Chemical Vapor Deposition (RF-PECVD) Technique, *Front. Mater. Sci. China*, 2009, **3**, p 409–414
12. V. Inkin, A Superhard Diamond-Like Carbon Film, *Diam. Relat. Mater.*, 2000, **9**, p 715–721
13. A. Grill, Electrical and Optical Properties of Diamond-Like Carbon, *Thin Solid Films*, 1999, **355–356**, p 189–193
14. B. Podgornik, M. Sedlacek, and J. Vizintin, Compatibility of DLC Coatings with Formulated Oils, *Tribol. Int.*, 2008, **41**, p 564–570
15. G. Zhang, P. Yan, P. Wang, Y. Chen, J. Zhang, and L. Wang, The Effect of Applied Substrate Negative Bias Voltage on the Structure and Properties of Al-Containing a-C:H Thin Films, *Surf. Coat. Technol.*, 2008, **202**, p 2684–2689
16. A. Escudeiro, T. Polcar, and A. Cavaleiro, Tribological Behaviour a-C and a-C:H Films Doped with Ti in Biological Solutions, *Vacuum*, 2011, **85**, p 1144–1148
17. M. Sasaki, Y. Kozukue, K. Hashimoto, K. Takayama, I. Nakamura, and I. Takano, Properties of Carbon Films with a Dose of Titanium or Zirconium Prepared by Magnetron Sputtering, *Surf. Coat. Technol.*, 2005, **196**, p 236–240
18. Y. Chang, Catalysis Effect of Metal Doping on Wear Properties of Diamond-Like Carbon Films Deposited by a Cathodic-Arc Activated Deposition Process, *Thin Solid Films*, 2002, **420–421**, p 241–247
19. D. Caschera, F. Federici, S. Kaciulis, L. Pandolfi, A. Cusma, and G. Padeletti, Deposition of Ti-containing diamond-like carbon (DLC) films by PECVD technique, *Mater. Sci. Eng., C*, 2007, **27**, p 1328–1330
20. Y.F. Zheng, X.L. Liu, and H.F. Zhang, Properties of Zr-ZrC-ZrC/DLC Gradient Films on TiNi Alloy by the PIII Technique Combined with PECVD, *Adv. Mater.*, 2008, **202**, p 3011–3016
21. J.C. Sanchez-Lopez and A. Fernandez, Doping and Alloying Effects on DLC Coatings, Chapter 12, *Tribology of Diamond-Like Carbon Films: Fundamentals and Applications*, A. Erdemir and C. Donnet, Ed., Springer, New York, 2008, p 311–338
22. W.H. Kao, Optimized a-C Coatings by Doping with Zirconium for Tribological Properties and Machining Performance, *Diam. Relat. Mater.*, 2007, **16**, p 1896–1904
23. C. Wei and J. Yen, Effect of Film Thickness and Interlayer on the Adhesion Strength of Diamond Like Carbon Films on Different Substrates, *Diam. Relat. Mater.*, 2007, **16**, p 1325–1330
24. Standard Test Method for Linearly Reciprocating Ball-on-Flat Sliding Wear, *ASTM G-133-02*
25. Y. Show, V.M. Swope, and G.M. Swain, The Effect of the CH_4 Level on The Morphology, Microstructure, Phase Purity and Electrochemical Properties of Carbon Films Deposited by Microwave-Assisted CVD from Ar-Rich Source Gas Mixtures, *Diam. Relat. Mater.*, 2009, **18**, p 1426–1434
26. X. Pang, L. Shi, P. Wang, Y. Xia, and W. Liu, Influence of Methane Flow on the Microstructure and Properties of TiAl-Doped a-C:H Films

- Deposited by Middle Frequency Reactive Magnetron Sputtering, *Surf. Int. Anal.*, 2009, **41**, p 924–930
27. F.C. Tai, S.C. Lee, J. Chen, C. Wei, and S.H. Chang, Multippeak Fitting Analysis of Raman Spectra on DLCH Film, *J. Raman Spectrosc.*, 2009, **40**, p 1055–1059
 28. A. Ferrari and J. Robertson, Origin of the 1150-cm^{-1} Raman Mode in Nanocrystalline Diamond, *Phys. Rev. B*, 2001, **63**, p 2–5
 29. A.C. Ferrari and J. Robertson, Interpretation of Raman Spectra of Disordered and Amorphous Carbon, *Phys. Rev. B*, 2000, **61**, p 95–107
 30. A.C. Ferrari, A Model to Interpret the Raman Spectra of Disordered Amorphous and Nanostructured Carbons, *Mater. Res.*, 2001, **675**, p 1–12
 31. G. Irmer and A. Dörner-Reisel, Micro-Raman Studies on DLC Coatings, *Adv. Eng. Mater.*, 2005, **7**, p 694–705
 32. F.-X. Liu, K.-L. Yao, and Z.-L. Liu, Different Substrate Materials Effect on Structure of ta-C Films by Raman Spectroscopy for Magnetic Recording Sliders, *J. Non-Cryst. Solids*, 2007, **353**, p 2545–2549